SEMARAK ILMU PUBLISHING

Journal of Advanced Research in Applied Sciences and Engineering Technology

Journal homepage:
https://semarakilmu.com.my/journals/index.php/applied_sciences_eng_tech/index
ISSN: 2462-1943

An Improved Variational-Based Model for Denoising and Segmentation of Vector-Valued Images

Nurhuda Ismail[1], Abdul Kadir Jumaat[2,3,*], Nurul Fatin Azara Zulkarnain[2]

[1] School of Mathematical Sciences, College of Computing, Informatics and Mathematics, Universiti Teknologi MARA, Johor Branch, Pasir Gudang Campus, 81750 Johor, Malaysia
[2] School of Mathematical Sciences, College of Computing, Informatics and Mathematics, Universiti Teknologi MARA, 40450 Shah Alam, Malaysia
[3] Institute for Big Data Analytics and Artificial Intelligence (IBDAAI), Universiti Teknologi MARA, 40450 Shah Alam, Malaysia

ARTICLE INFO

Article history:
Received 22 June 2023
Received in revised form 2 September 2023
Accepted 21 October 2023
Available online 19 February 2024

Keywords:
Vector-Valued Image Processing; Denoising; Segmentation; Total Variation

ABSTRACT

Preserving important features such as edges is one of the main concerns in models for denoising and segmenting vector-valued (colour) images. The Rudin-Osher-Fatemi (ROF) model is a well-known variational-based image denoising model that is capable of reducing image noise while preserving image edges. However, the ROF model is not formulated for denoising colour images and is less effective in preserving corners and weak edges. On the other hand, a variational-based selective segmentation model for colour images called the selective distance segmentation (DSS2) model has recently been proposed, which can effectively partition or extract a specific object in an image. However, the DSS2 model has problems in segmenting colour images with noise, which may result in poor segmentation. Therefore, in this research, we first modify the ROF model to denoise vector-valued images by including the edge detector and extending the formulation into a vector-valued framework. Second, we reformulate the DSS2 model by incorporating the modified ROF model as a new fitting term in the DSS2 model. Peak signal-to-noise ratio (PSNR) is used to measure the image quality, while Jaccard and Dice similarity index are used to evaluate the segmentation quality. The comparison between our proposed model and existing model shows that our model is more effective as indicated by higher PSNR, Jaccard and Dice similarity index values.

1. Introduction

Digital images can be obtained using various techniques and input devices such as scanners, digital cameras and others. The output can be binary, grayscale or vector-valued images. Vector-valued digital images, or colour images, have a considerable wealth of information that provides better meaning of image features such as edges. To facilitate interpretation or enhance information from colour images, image processing steps have been performed by Torres *et al.,* [1]. The most common image processing tasks are image segmentation and image denoising.

Image segmentation is a technique used to extract the boundaries of an object or to divide an image into multiple segments, according to the authors [2-4]. Once the boundary of the target object

* *Corresponding author.*
E-mail address: abdulkadir@tmsk.uitm.edu.my

https://doi.org/10.37934/araset.40.1.189203

has been segmented, it is further analysed. In medicine, for example, it is used to analyse the nature of diseases such as cancer and breast abnormalities, as done by several authors [5-10]. Different models are used for image segmentation, which can be divided into two categories, namely the non-variational and variational approaches.

The non-variational model is a category in which the image segmentation processes are mostly performed using a learning-based method which include the Convolutional Neural Networks proposed by Moon *et al*., [11] and the U-Net framework used by Amiri *et al*., [12]. As reported by Masood *et al*., in [13], studies have demonstrated the efficacy of these learning-based techniques in non-variational image segmentation. According to Lee *et al*., [14], the machine learning based approach also has its drawbacks, e.g., it is highly data dependent, and the process of image segmentation is unknown. Other methods of non-variational image segmentation that are not based on machine learning are the region expanding and thresholding methods proposed by the authors [15,16], respectively. As authors [17-19] point out, the region expanding and thresholding procedures have the potential to give poor results for a target region that has low contrast, noisy pictures, and is adjacent to an item in the surrounding area.

In variational image processing, an image is considered as a feature whose sampling corresponds to the discrete matrix form of a given image. Various studies summarised by Dobrosotskaya and Guo [20] have shown that variational image segmentation methods are effective and capable of providing high-quality image processing functions. For example, variational models derived using a level set framework can adapt to topological changes in an input image and are less sensitive to initialisations, as mentioned by the authors [19,21].

The use of variational models for segmentation may be broken down into two distinct categories: selective segmentation and global segmentation. The global segmentation model is a strategy that may be used to separate all of the items that are present in a picture based on specific attributes. Several writers [21-25] have come up with a variety of approaches for global segmentation. According to Abdullah and Jumaat [3] global segmentation methods are successful at separating all of the items included in digital pictures; but they are far less effective when it comes to isolating only one specific object from any given image.

Selective segmentation is about extracting specific regions and features of the image under consideration, as explained by the authors [2,3]. This is often used in medical image analysis, for example, to extract anatomical organs or lesions. Examples of effective selective models are proposed by several authors [3,17-19,26]. However, all of these models are not designed for the segmentation of colour images. The variational selective segmentation model for colour images was recently proposed by Ghani and Jumaat [4] and named as Distance Selective Segmentation 2 (DSS2) model. However, the DSS2 model can be sensitive to image noise. Therefore, some modifications to the DSS2 model are required to improve its segmentation accuracy. In this study, we propose to modify the DSS2 model using image denoising techniques.

Image denoising is a process of reducing the amount of noise in a digital image while preserving the true image. The non-linear filters can preserve important aspects in the denoised image, especially the edges. According to Bresson *et al*., [27], one of the most popular and influential nonlinear filters is the seminal work of Rudin *et al*., [28], referred to as Rudin, Osher and Fatemi's (ROF) model. The ROF model is currently cited more than 17,000 times in the Google scholar database and more than 12,000 times in the Scopus database. As a nonlinear filter with a variational-based formulation, the ROF model is able to reduce image noise while preserving image edges. However, the ROF model is not formulated for denoising colour images and, according to the author, is less effective at preserving corners and weak edges [27].

In this study, we first modify the ROF model to denoise vector-valued images by incorporating the edge detector function to preserve the image corners and weak edges. We also extend the formulation into a vector-valued framework. Second, we reformulate the DSS2 model by including the modified ROF model as a new fitting term in the DSS2 model. We anticipate that altering the ROF model and the DSS2 model will result in improvements in terms of both the picture quality and the accuracy of the segmentation.

The next part of this article offers a concise review of the models associated with this study, which is then followed by the model's formulations. After that, the results of the experiments conducted on both the current models and the suggested models are provided.

2. Review on the ROF Model and DSS2 Model

The ROF model minimizes the total variation of the image subject to constraints that affect the statistics of the noise. The constraints are exploited using Lagrange multipliers, while the solution is obtained using the gradient projection method. The Euler-Lagrange equation associated with the ROF model is discretized using a finite difference scheme with fixed points. The model proposes to minimize the following Eq. (1):

$$\min_{z_{ROF}} F(z_{ROF}) = \lambda \int_D |f - z_{ROF}|^2 \, dD + \int_D |\nabla z_{ROF}| \, dD. \tag{1}$$

where D is the domain of the noisy input image, $f = f(x,y)$, z_{ROF} is the unknown clean image, and $l > 0$ is a scaling parameter. The corresponding Euler-Lagrange equation of the ROF model is formally defined as the following Eq. (2):

$$z_{ROF} = f + \frac{1}{2\lambda} div\left(\frac{\nabla z_{ROF}}{|\nabla z_{ROF}|}\right). \tag{2}$$

The gradient descent method was used to solve Eq. (2).

Ghani and Jumaat [4] presented a modern variational-based selective segmentation for a colour picture. This model, which they referred to as Distance Selective Segmentation 2 (DSS2), was developed for selective segmentation. Let $z_0 = z_0(x,y)$ be the input digital image in domain D. In the DSS2 model, z_0 is formed by two homogeneous regions, where contour γ separates the regions. The region D_1 represents the specific object with intensity value b_1 inside the curve γ while the image intensity value b_2 in the region $D_2 = D \setminus D_1$ which is outside the curve γ. The curve γ is defined as the zero-level set function, $\phi(x,y)$ i.e. $\gamma = \{(x,y) \in D | \phi(x,y) = 0\}$. They introduced a marker set $A = \{w_j = (x_j^*, y_j^*) \in D, 1 \le j \le n_1\}$ with n_1(≥3) points near the targeted object. The Euclidean distance function $E_d(x,y) = \sqrt{(x - x_p)^2 + (y - y_p)^2}$ of each point $(x,y) \in D$ is defined from its nearest point in the polygon, P made up of $(x_p, y_p) \in P$, constructed from A. Then, with $D = D_1 \cup D_2$, the DSS2 function is defined as the following Eq. (3):

$$\min_{\phi, c_1^i, c_2^i} DSS2(\phi, c_1^i, c_2^i) = \int_D \delta(\phi) |\nabla \phi| dD + \int_D r dD + \int_D \theta H(\phi) P_d dD. \tag{3}$$

Here, $r=\frac{1}{N}\left[\sum_{i=1}^{N}\left(1-H(\phi)\right)\left(z_0^i-c_2^i\right)^2+\sum_{i=1}^{N}H(\phi)\left(z_0^i-c_1^i\right)^2\right]$ where $i=1,2...N$ are the colour channels ($N=3$ for Red, Green and Blue). Both c_1^i and c_2^i are unknown constants that indicate the average value of input colour image z_0^i inside and outside of the unknown curve, respectively. In Eq. (3), the first term is referred to as the regularizing term, the second term is known as the fitting term, and the third term is known as the distance function term. The distance function has a weight that is denoted by the constant q. Following the introduction of the Heaviside function, $H\left(\phi(x,y)\right)$, and the Dirac delta function, $\delta\left(\phi(x,y)\right)$, the following Euler-Lagrange Eq. (4), which is connected with the previous Eq. (3), is defined as follows:

$$\delta(\phi)\nabla.\left(\frac{\nabla\phi}{|\nabla\phi|}\right)-\delta(\phi)\frac{1}{N}\sum_{i=1}^{N}\left(z_0^i-c_1^i\right)^2+\delta(\phi)\frac{1}{N}\sum_{i=1}^{N}\left(z_0^i-c_1^i\right)^2-\theta P_d=0. \tag{4}$$

The solution to Eq. (4) was found by combining the gradient descent method and the finite difference technique.

The ROF model and the DSS2 model discussed above are considered as the basis for our proposed models. We find that the ROF model is the origin of many variational models as a powerful nonlinear filter with variational-based formulation capable of reducing image noise while preserving image edges. However, the ROF model is not formulated for denoising colour images and, according to the author [27], is less effective in preserving corners and weak edges. On the other hand, although the DSS2 model is effective in segmenting colour images, it can be sensitive to image noise and therefore give unsatisfactory results in segmenting noisy images. Therefore, some modifications of the ROF model and the DSS2 model are required to improve their accuracy. In the next section, the methodology for modifying the ROF model and the SSCD model is presented.

3. Methodology

In this section we demonstrate the methodology for modifying the ROF model and the DSS2 model.

3.1 Modified ROF Model

The ROF model in Eq. (1) can be extended into vector-valued environment. First, we defined N as the number of channels for colour component where normally $N=3$ that represent 3 colour channels (Red, Green and Blue). Hence, the modified ROF model, termed M_1 model in vector-valued framework can be defined as the following Eq. (5):

$$\min_{z_{ROF}} M_1(z_{ROF})=\int_D\frac{1}{2\lambda}\sum_{i=1}^{N}|f^i-z_{ROF}^i|^2\,dD+\int_D\sum_{i=1}^{N}\left|\nabla z_{ROF}^i\right|dD \tag{5}$$

Next, we incorporate the edge detection function in the Eq. (5) to give another variant of the modified ROF model, M_2 defined as the following Eq. (6):

$$\min_{z_{ROF}} M_2(z_{ROF}) = \int_D \frac{1}{2\lambda} \sum_{i=1}^{N} | f^i - z_{ROF}^i |^2 \, dD + \int_D \sum_{i=1}^{N} g^i \left| \nabla z_{ROF}^i \right| dD. \tag{6}$$

where $g^i = \dfrac{1}{1 + b\left|\nabla f\right|}$ is an edge detection function that approaches to zero at object verges and b is an arbitrary positive constant. Inspired by the work from Bresson *et al*., [27], the modified M_1 and M_2 models can be solved by using projection method, with a semi-implicit gradient descent scheme. Here, we only demonstrate how to solve M_2 of Eq. (6) because the method to solve M_1 model is mostly the same (without the function g^i). Initially, Eq. (6) can be written in dual variable $p^i = (p_1^i, p_2^i)$:

$$\max_{|p^i| \le g^i} \min_{z_{ROF}^i} \int_D \frac{1}{2\lambda} \sum_{i=1}^{N} | f^i - z_{ROF}^i |^2 dD + \int_D \sum_{i=1}^{N} z_{ROF}^i \, \nabla \cdot p^i \, dD. \tag{7}$$

By Calculus of Variation, we obtain the following Euler Lagrange Equation:

$$f^i - z_{ROF}^i - \lambda \nabla \cdot p^i = 0 \Rightarrow z_{ROF}^i = f^i - \lambda \nabla \cdot p^i \;,\; 1 \le i \le N. \tag{8}$$

Substituting the Eq. (8) for minimal u into the max-min problem in Eq. (7) provides $\max_{|p^i| \le g^i} \int_D \sum_{i=1}^{N} \left(f^i - z_{ROF}^i \nabla \cdot p^i \right) \nabla \cdot p^i + \frac{\lambda}{2} \left(\nabla \cdot p^i \right)^2 dD$ which can be simplified as the following Eq. (9):

$$\int_D \sum_{i=1}^{N} f^i \nabla \cdot p^i - \frac{\lambda}{2} \left(\nabla \cdot p^i \right)^2 dD \tag{9}$$

Variations of Energy in (9) with respect to the vector field p give $\int_D \sum_{i=1}^{N} \left(-\nabla f^i + \lambda \nabla \cdot \nabla \cdot p^i \right) \cdot \delta p^i \, dD$. We can get the necessary optimality condition, along with the point-wise constraint $\left|p^i\right|^2 - \left(g^i\right)^2 \le 0$ as:

$$-\nabla \left(\lambda \nabla \cdot p^i - f^i \right) + \alpha p^i = 0. \tag{10}$$

Here, $a(x) \ge 0$ is the Lagrange multiplier. If $\left|p^i\right|^2 < \left(g^i\right)^2$, then the Lagrange multiplier is not active, hence $a = 0$ and if $\left|p^i\right|^2 = \left(g^i\right)^2$, then the Lagrange multiplier is active, hence

$$\left| \nabla \left(\lambda \nabla \cdot p^i - f^i \right) \right|^2 - \alpha^2 \left(g^i \right)^2 = 0 \tag{11}$$

In conclusion, in either case, the value of $a(x)$ is given as $\alpha = \frac{1}{g^i} | \nabla (\lambda \nabla \cdot p^i - f^i) |$. Upon substituting into Eq. (10), we get the following Eq. (12):

$$\nabla(\lambda\nabla\cdot p^i - f^i) - \frac{1}{g^i}|\nabla(\lambda\nabla\cdot p^i - f^i)|\,p^i = 0 \tag{12}$$

By using a semi-implicit gradient descent algorithm, we reach the following Eq. (13):

$$\left(p^i\right)^{n+1} = \frac{\left(p^i\right)^n + \delta t\nabla\left(\nabla\cdot\left(p^i\right)^n - f^i/\lambda\right)}{1+\frac{\delta t}{g^i}\left|\nabla(\lambda\nabla\cdot\left(p^i\right)^n - f^i/\lambda)\right|} \tag{13}$$

Similarly, the semi-implicit gradient descent algorithm for M_1 is defined as the following Eq. (14):

$$\left(p^i\right)^{n+1} = \frac{\left(p^i\right)^n + \delta t\nabla\left(\nabla\cdot\left(p^i\right)^n - f^i/\lambda\right)}{1+\delta t\left|\nabla(\lambda\nabla\cdot\left(p^i\right)^n - f^i/\lambda)\right|} \tag{14}$$

This following Algorithm 1 shows the steps involved to implement the modified ROF model, M_2.

Algorithm 1: Algorithm to solve the proposed M_2 model.

1. Use the command 'imread' in MATLAB to import the noisy image.
2. Set the parameter values of $\delta t = 1/8$ and vary the value λ depending on the input image (large λ for image with high noise amount).
3. Initialize $n=0$, thus $\left(z_{ROF}^i\right)^{n=0} = 0$ and $\left(p^i\right)^{n=0} = 0$
4. **For** $iter = 1$ to maximum iterations, *maxiter* or $\frac{\left\|z_{ROF}^{i,n+1} - z_{ROF}^{i,n}\right\|}{\left\|z_{ROF}^{i,n}\right\|} \le tol$ **do**

   Calculate $\left(p^i\right)^n$ of Eq. (13).

   Update $\left(z_{ROF}^i\right)^n$ of Eq. (8)

   end for
5. The output z_{ROF}^i will be defined as the final solution.

Here we have used the value of tolerance, $tol = 1 \times 10^{-16}$, and the maximum number of iterations (*maxiter*) is 100 iterations. By changing Eq. (13) with Eq. (14), a similar process is repeated for the implementation of the M_1 model. The steps for implementing the modified ROF model, M_1 can thus be summarised as the following Algorithm 2.

Algorithm 2: Algorithm to solve the proposed M_1 model

1. Input all the parameters setting as in Algorithm 1
2. Apply Algorithm 1 to functional of Eq. (5) from replacing Eq. (13) by Eq. (14)

All other steps are identical.

An experiment will be conducted to decide which modified version of the ROF model gives better results. To formulate the modified DSS2 model, the information from the chosen modified ROF model is integrated into the original DSS2 model.

3.2 Modified DSS2 Model

The DSS2 model proposed by Ghani and Jumaat [4] is modified by substituting the fitting term, z_0^i in Eq. (3) with z_{ROF}^i generated from the chosen modified ROF model. The modified DSS2 model, called *MDSS*2 model is defined as the following Eq. (15):

$$\begin{aligned}&\min_{\phi,c_1^i,c_2^i}\left\{MDSS2\left(\phi,c_1^i,c_2^i\right)=\mu\int_D\delta(\phi)|\nabla\phi|dD+\int_D\frac{1}{N}\sum_{i=1}^{N}\left(1-H(\phi)\right)\left(z_{ROF}^i-c_2^i\right)^2dD\right.\\&\left.+\int_D\frac{1}{N}\sum_{i=1}^{N}H(\phi)\left(z_{ROF}^i-c_1^i\right)^2dD\ +\int_D\theta H(\phi)P_d\,dD\right\}.\end{aligned}\tag{15}$$

It is possible to demonstrate, via the use of the Calculus of Variations, that the relevant Euler Lagrange equation of the model is specified by the Eq. (16) that is shown here:

$$\begin{cases}\delta(\phi)\nabla.\left(\dfrac{\nabla\phi}{|\nabla\phi|}\right)-\delta(\phi)\dfrac{1}{N}\displaystyle\sum_{i=1}^{N}\left(z_{ROF}^i-c_1^i\right)^2+\delta(\phi)\dfrac{1}{N}\sum_{i=1}^{N}\left(z_{ROF}^i-c_1^i\right)^2-\theta P_d=0, & in\ \mathrm{D},\\ \dfrac{\delta(\phi)}{|\nabla\phi|}\dfrac{\partial\phi}{\partial\vec{n}}=0, & on\ \partial D.\end{cases}\tag{16}$$

To solve the Eq. (16), we consider the gradient descent flow that represent the evolution of the unknown curve $f(x,y)$ as follows:

$$\begin{cases}\dfrac{\partial\phi}{\partial t}=\delta(\phi)\left[\mathrm{div}\left(\dfrac{\nabla\phi}{|\nabla\phi|}\right)-\dfrac{1}{N}\left[\displaystyle\sum_{i=1}^{N}\left(z_{ROF}^i-c_1^i\right)^2-\frac{1}{N}\sum_{i=1}^{N}\left(z_{ROF}^i-c_2^i\right)^2\right]-\theta P_d\right] & \text{in D},\\ \dfrac{\delta(\phi)}{|\nabla\phi|}\dfrac{\partial\phi}{\partial\vec{n}}=0 & \text{on } \partial D,\end{cases}\tag{17}$$

Subsequently, the Eq. (17) can be solved iteratively using a finite difference scheme with Neumann boundary condition. The procedures necessary to compute the answer using the newly suggested model *MDSS*2 are outlined in the following Algorithm 3.

Algorithm 3: Algorithm to solve the proposed *MDSS*2 model.

1. Use the command 'imread' in MATLAB to import the image.
2. Set the parameter values of θ and marker set *A*.
3. Compute the solution of the function E_d and the functional z_{ROF}^i.
4. Initialize ϕ^0, $n = 0$.
5. **For** $iter = 1$ to maximum iterations, *maxit* or $\dfrac{\left\|\phi^{n+1}-\phi^n\right\|}{\left\|\phi^n\right\|}\le tol$ **do**

Calculate the average intensity values $c_1^i\left(\phi^n\right)$ and $c_2^i\left(\phi^n\right)$

Solve for ϕ^n in Eq. (16) to obtain ϕ^{n+1}.

end for

6. The output ϕ will be defined as the final solution.

Here, we used the value of tolerance, $tol = 1 \times 10^{-4}$ and the maximum number of iterations (*maxit*) is 500 iterations.

4. Results and Discussion

In this section, we first compared the denoising quality of the modified ROF models, i.e., the M_1 model and the M_2 model, using the peak signal-to-noise ratio (PSNR). The values of l range from 60 to 100. Figure 1 shows the test images of size $128¥128$ and the results produced by the two modified models.

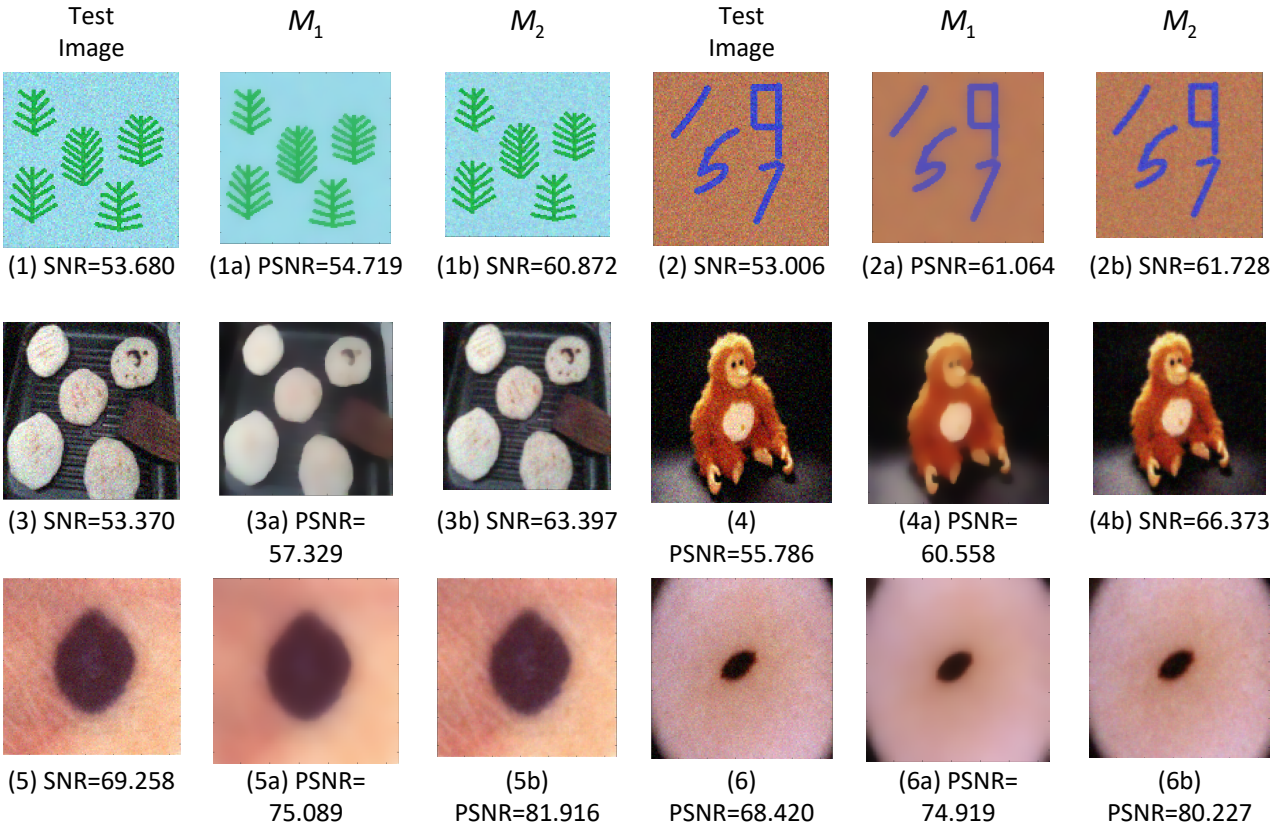

Fig. 1. The test images and the denoising results from the M_1 model and the M_2 model

Based on Figure 1, the first and fourth columns represent the noisy test images with their respective PSNR values. Images (1) and (2) were self-generated synthetic images. The real images (3) and (4) were taken from the authors' datasets [29,30], respectively. The medical images (5) and (6) were from the public dataset created by the authors [31]. The second and fifth columns show the denoising results with the PSNR values generated by the M_1 model, while the third and last columns show the denoising results with the PSNR values of the M_2 model. Visual inspection shows that both

models are able to reduce image noise. However, it is noticeable that the output of the M_1 model is blurrier compared to the M_2 model.

To investigate this quantitatively, we record the PSNR values for each output produced by the two modified models. For all test images, the M_2 model achieved higher PSNR values compared to the M_1 model. So, the M_2 model is better at reducing noise in the colour images. Thank you to the edge detector function included in the formulation of the M_2 model, important information of the image such as corners and weak edges can be preserved.

In the next experiment, we compared the performance of the original DSS2 model with that of the proposed MDSS2 model. Here, we chose the output of the M_2 model to be included in the fitting term of the MDSS2 model. Figure 2 shows the self-generated synthetic test images with the marker set indicating the target object and the results for each model in curve and binary representation. All images are of size $128 \text{¥} 128$ unless otherwise stated.

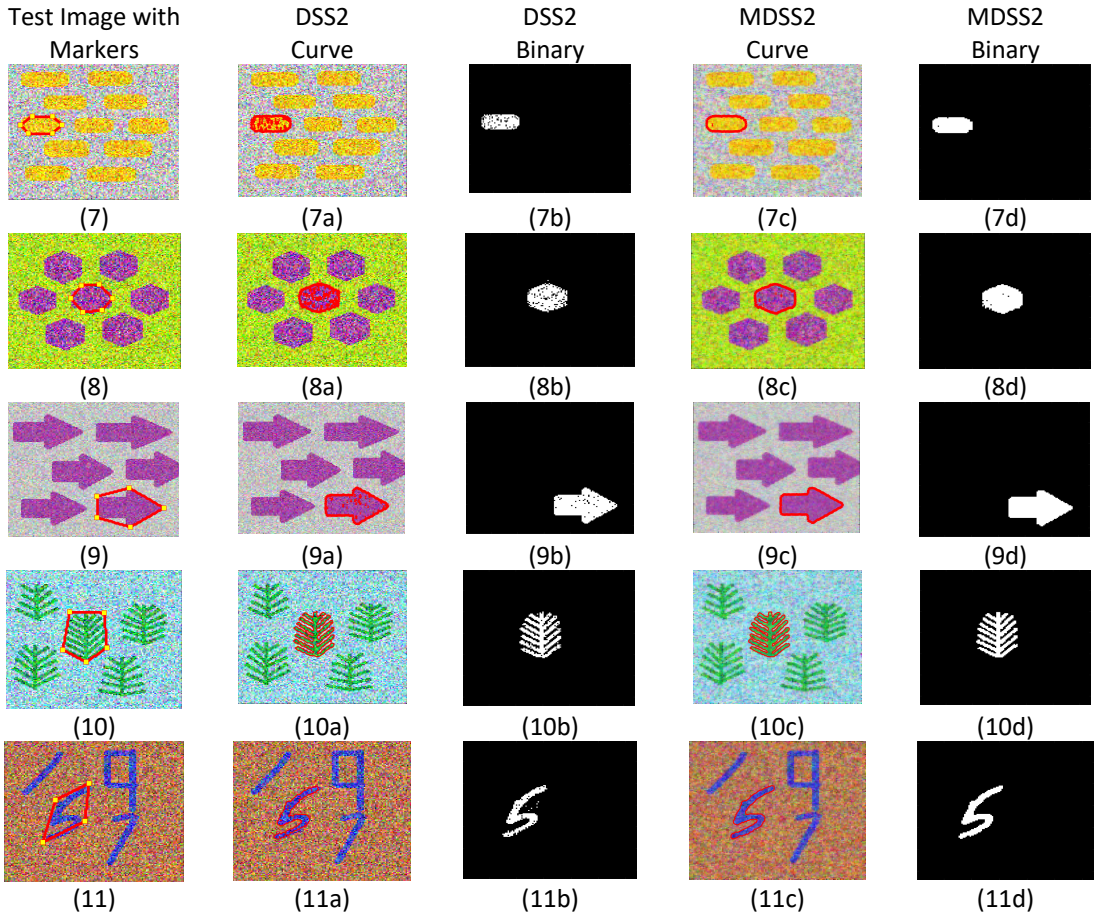

Fig. 2. Segmentation results of the DSS2 model and the MDSS2 model in segmenting synthetic images

The self-generated synthetic test images with the marker set are shown in the first column of Figure 2. The second column and the fourth column show the results in curve representation for the DSS2 model and the MDSS2 model, respectively. The third and last columns show the segmentation results in binary representation for the DSS2 model and the MDSS2 model, respectively.

By visual observation, both models are able to segment the target object. However, the curve generated by the MDSS2 model is smoother than that of the original DSS2 model. Furthermore, the DSS2 model segments many noise particles within the target object compared to the MDSS2 model.

Moreover, the results of the MDSS2 model are cleaner than those of the DSS2 model. These observations indicate the denoising effect used in the formulation of MDSS2, while the DSS2 model does not contain any denoising element.

To evaluate the segmentation accuracy quantitatively, we compute the Jaccard (JSI) and Dice Similarity Index (DSI) as given by the following formulae: $JSI = |S_n \cap S_*| / |S_n \cup S_*|$ and $DSI = 2|S_n \cap S_*| / |S_n| + |S_*|$. Here, the set of the segmented domain D_1 is denoted by S_n while the true set of D_1 is denoted by S_*. The return values of JSI and DSI were in the range of $[0,1]$. A perfect segmentation quality is indicated by a value of 1 while poor quality of segmentation is indicated by a value of 0. The PSNR values of the results are recorded as well. The values of PSNR, JSI and DSI are tabulated in the following Table 1.

Table 1
The PSNR, JSI and DSI values for DSS2 model and MDSS2 model in segmenting synthetic images

Test Image	PSNR		JSI		DSI	
	DSS2	MDSS2	DSS2	MDSS2	DSS2	MDSS2
7	33.208	44.979	0.849	0.962	0.919	0.981
8	32.956	45.115	0.835	0.960	0.910	0.979
9	45.979	58.131	0.962	0.992	0.981	0.996
10	33.287	43.553	0.927	0.968	0.962	0.984
11	33.123	45.834	0.843	0.954	0.915	0.976

From Table 1, we can see that the PSNR values for our MDSS2 are higher than for the DSS2 for all test images. This shows that the MDSS2 produces cleaner results compared to the DSS2 model. Consequently, this contributes to the high JSI and DSI values in our proposed modified MDSS2 model. Thus, the image quality and segmentation accuracy of the MDSS2 model are better than those of the DSS2 model.

Besides the synthetic images, we are interested in comparing the performance of the DSS2 and MDSS2 models in segmenting real images, which are more challenging compared to the synthetic images used above. This is because the real images consist of a variety of intensities with many features. Figure 3 shows the real images (12)-(15), which are from the above sources and have been distorted by noise. The image (16) with the size 200×200 was taken from the mammography image database [32] and given a yellow colour map to highlight the mass-like patterns.

The first column of Figure 3 shows the test images with set markers indicating the target region. The results in the curve plot are shown in the second column and the fourth column for the DSS2 model and the MDSS2 model, respectively, while the results in the binary plot are shown in the third and last column for the DSS2 model and the MDSS2 model, respectively.

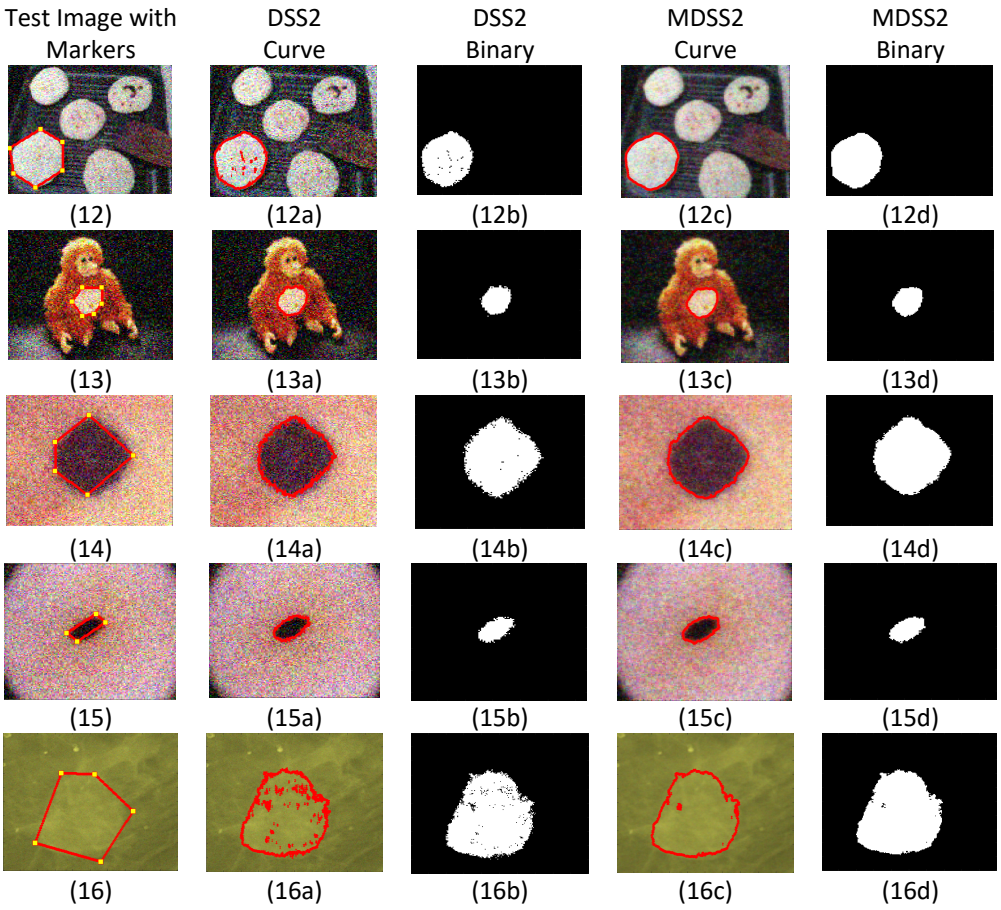

Fig. 3. Segmentation results of the DSS2 model and the MDSS2 model in segmenting real images

From the results, it can be seen that both models can segment the target object. However, both models show similar behaviour to the previous experiment with synthetic images, where the curve generated by the MDSS2 model is smoother and cleaner than the original DSS2 model. We can see that the DSS2 model segments a lot of image noise compared to the MDSS2 model, as the DSS2 formulation does not include an image denoising element. To confirm the results quantitatively, we record the PSNR, JSI and DSI values in Table 2 below.

Table 2 shows that the PSNR, JSI and DSI values of the proposed MDSS2 model are higher than those of the original DSS2 model for all the images tested. These results show the advantage of using the denoising information from the proposed M_2 denoising model in the MDSS2 formulation.

Table 2
The PSNR, JSI and DSI values for DSS2 model and MDSS2 model in segmenting real images

Test Image	PSNR		JSI		DSI	
	DSS2	MDSS2	DSS2	MDSS2	DSS2	MDSS2
12	36.051	48.191	0.846	0.866	0.917	0.928
13	37.803	48.734	0.905	0.918	0.950	0.957
14	38.143	51.909	0.848	0.899	0.918	0.947
15	37.658	51.019	0.844	0.911	0.916	0.953
16	72.495	86.510	0.839	0.858	0.912	0.924

We note that by including the information from the M_2 model in the MDSS2 formulation, the processing time for the MDSS2 is slower than for the original DSS2 model. This is highlighted in Table 3 below.

Table 3 shows that the processing time for the MDSS2 model is about 2-5 seconds slower than for the DSS2 model. This is to be expected as the combination of the M_2 model with the DSS2 model to create the MDSS2 model results in a high computational complexity. Therefore, the processing time for solving the MDSS2 model is longer than that of the DSS2 model. This observation also shows the major limitation of our proposed MDSS2 model. Despite this limitation, the MDSS2 model has high potential in many research areas such oil and gas industries [33] for corrosion detection, ultrasound imaging in biofuel production [34] and it can be integrated with artificial neural network [35] for image processing.

Table 3
The processing time taken by DSS2 model and MDSS2 model

Test Image	Time		Test Image	Time	
	DSS2	MDSS2		DSS2	MDSS2
7	15.690	20.122	12	17.045	20.411
8	16.671	20.612	13	16.868	20.028
9	17.360	19.627	14	17.821	19.878
10	17.260	20.473	15	16.707	19.522
11	16.606	20.020	16	19.848	22.638

4. Conclusions

In this research paper, we focus on two main issues in colour image processing, namely noise reduction of colour images and segmentation of colour images in the context of variational techniques. One of the most influential variational-based models for image denoising is the ROF model, as it effectively reduces image noise while preserving important features such as edges. However, the ROF model is not formulated for denoising colour images and is less effective in preserving corners and weak edges. Therefore, we have formulated the ROF model and recommend a modified version of the ROF model called the M_2 model. We have described how the M_2 model can be solved using a projection algorithm with a semi-implicit gradient descent scheme. Based on numerical experiments with synthetic and real images, the M_2 model, which uses the edge detector in a vector-valued environment, produces high image quality as indicated by the PSNR value compared to the other modified model, M_1. These results show the advantage of using the edge detector in the formulation of the M_2 model, which can help to preserve weak edges.

For colour image segmentation, we have proposed a modified variational-based selective segmentation, referred to as MDSS2, based on the recent variational-based Distance Selective Segmentation (DSS2) model. The modification of the original DSS2 model was done by incorporating the information from the M_2 model as a new fitting term in the DSS2 model. We established the Euler-Lagrange equation of the MDSS2 model and proposed to solve it using a finite difference approach. In the experiments conducted with synthetic and real images, the proposed MDSS2 model yields high values of PSNR, JSI and DSI index. This indicates that the MDSS2 model has better image quality and segmentation accuracy compared to the original DSS2 model. Again, the advantage of including image denoising in the image segmentation formulation to achieve good results is evident.

For further investigation, the recommended models i.e., M_2 model and MDSS2 model can be extended to other applications such as food image processing. It can also be reformulated into a three-dimensional framework. The reason for this is that three-dimensional images contain a wealth of information that can be helpful in the analysis of digital images.

Acknowledgement
This work was supported by the Ministry of Higher Education (MOHE) and Universiti Teknologi MARA, Shah Alam, grant number FRGS/1/2021/STG06/UITM/02/3.

References

[1] Torres, Helena R., Pedro Morais, Bruno Oliveira, Cahit Birdir, Mario Rüdiger, Jaime C. Fonseca, and João L. Vilaça. "A review of image processing methods for fetal head and brain analysis in ultrasound images." *Computer Methods and Programs in Biomedicine* 215 (2022): 106629. https://doi.org/10.1016/j.cmpb.2022.106629

[2] Mohd Ghani, Noor Ain Syazwani, Abdul Kadir Jumaat, and Rozi Mahmud. "Boundary extraction of abnormality region in breast mammography image using active contours." *ESTEEM Academic Journal* 18 (2022): 115-127.

[3] Abdullah, Siti Aminah, and Abdul Kadir Jumaat. "Selective image segmentation models using three distance functions." *Journal of Information and Communication Technology* 21, no. 01 (2022): 95-116. https://doi.org/10.32890/10.32890/jict2022.21.1.5

[4] Mohd Ghani, Noor Ain Syazwani, and Abdul Kadir Jumaat. "Selective Segmentation Model for Vector-Valued Images." *Journal of Information and Communication Technology* 21, no. 02 (2022): 149-173. https://doi.org/10.32890/jict2022.21.2.1

[5] Zaman, Nur Atiqah Kamarul, Wan Eny Zarina Wan Abdul Rahman, Abdul Kadir Jumaat, and Siti Salmah Yasiran. "Classification of breast abnormalities using artificial neural network." In *AIP Conference Proceedings*, vol. 1660, no. 1. AIP Publishing, 2015. https://doi.org/10.1063/1.4915671

[6] Jumaat, Abdul Kadir, Siti Salmah Yasiran, Aminah Abdul Malek, Wan Eny Zarina WA Rahman, Norzaituleha Badrin, Siti Hajar Osman, Siti Rohaina Rafiee, and Rozi Mahmud. "Performance comparison of Canny and Sobel edge detectors on Balloon Snake in segmenting masses." In *2014 International Conference on Computer and Information Sciences (ICCOINS)*, pp. 1-5. IEEE, 2014. https://doi.org/10.1109/ICCOINS.2014.6868368

[7] Jumaat, Abdul K., Wan E. Rahman, Arsmah Ibrahim, Siti S. Yasiran, Rozi Mahmud, and Aminah A. Malek. "Masses characterization based on angular margin measurement." In *2012 Fourth International Conference on Computational Intelligence, Modelling and Simulation*, pp. 265-269. IEEE, 2012. https://doi.org/10.1109/CIMSim.2012.50

[8] Jumaat, Abdul Kadir, Wan Eny Zarina WA Rahman, Arsmah Ibrahim, and Rozi Mahmud. "Segmentation and characterization of masses in breast ultrasound images using active contour." In *2011 IEEE International Conference on Signal and Image Processing Applications (ICSIPA)*, pp. 404-409. IEEE, 2011. https://doi.org/10.1109/ICSIPA.2011.6144126

[9] Yasiran, Siti Salmah, Abdul Kadir Jumaat, Aminah Abdul Malek, Fatin Hanani Hashim, Nor Dhaniah Nasrir, Syarifah Nurul Azirah Sayed Hassan, Normah Ahmad, and Rozi Mahmud. "Microcalcifications segmentation using three edge detection techniques." In *2012 IEEE International Conference on Electronics Design, Systems and Applications (ICEDSA)*, pp. 207-211. IEEE, 2012. https://doi.org/10.1109/ICEDSA.2012.6507798

[10] Yasiran, Siti Salmah, Abdul Kadir Jumaat, Mazani Manaf, Arsmah Ibrahim, WAR Wan Eny Zarina, Aminah Malek, Mohamed Faris Laham, and Rozi Mahmud. "Comparison between GVF snake and ED snake in segmenting microcalcifications." In *2011 IEEE International Conference on Computer Applications and Industrial Electronics (ICCAIE)*, pp. 597-601. IEEE, 2011. https://doi.org/10.1109/ICCAIE.2011.6162204

[11] Moon, Woo Kyung, Yan-Wei Lee, Hao-Hsiang Ke, Su Hyun Lee, Chiun-Sheng Huang, and Ruey-Feng Chang. "Computer-aided diagnosis of breast ultrasound images using ensemble learning from convolutional neural networks." *Computer methods and programs in biomedicine* 190 (2020): 105361. https://doi.org/10.1016/j.cmpb.2020.105361

[12] Amiri, Mina, Rupert Brooks, Bahareh Behboodi, and Hassan Rivaz. "Two-stage ultrasound image segmentation using U-Net and test time augmentation." *International journal of computer assisted radiology and surgery* 15 (2020): 981-988. https://doi.org/10.1007/s11548-020-02158-3

[13] Masood, Saleha, Muhammad Sharif, Afifa Masood, Mussarat Yasmin, and Mudassar Raza. "A survey on medical image segmentation." *Current Medical Imaging* 11, no. 1 (2015): 3-14. https://doi.org/10.2174/1573405611011504231034 41

[14] Lee, Lay Khoon, Siau Chuin Liew, and Weng Jie Thong. "A review of image segmentation methodologies in medical image." In *Advanced Computer and Communication Engineering Technology: Proceedings of the 1st International Conference on Communication and Computer Engineering*, pp. 1069-1080. Springer International Publishing, 2015. https://doi.org/10.1007/978-3-319-07674-4_99

[15] Jiang, Xue, Yanhui Guo, Haibin Chen, Yaqin Zhang, and Yao Lu. "An adaptive region growing based on neutrosophic set in ultrasound domain for image segmentation." *IEEE Access* 7 (2019): 60584-60593. https://doi.org/10.1109/ACCESS.2019.2911560

[16] Ifan Roy Thanaraj, R., B. Anand, J. Allen Rahul, and V. Rajinikanth. "Appraisal of breast ultrasound image using Shannon's thresholding and level-set segmentation." In *Progress in Computing, Analytics and Networking: Proceedings of ICCAN 2019*, pp. 621-630. Springer Singapore, 2020. https://doi.org/10.1007/978-981-15-2414-1_62

[17] Chen, K., and A. Jumaat. "An Optimization Based Multilevel Algorithm for Variational Image Segmentation Models." *Electronic Transactions on Numerical Analysis* 46 (2017): 474-504.

[18] K Jumaat, Abdul, and Ke Chen. "Fast algorithm for selective image segmentation model." *International Journal of Engineering & Technology* 7, no. 4.33 (2018): 41-41. https://doi.org/10.14419/ijet.v7i4.33.23481

[19] Jumaat, Abdul K., and Ke Chen. "A reformulated convex and selective variational image segmentation model and its fast multilevel algorithm." *NUMERICAL MATHEMATICS-THEORY METHODS AND APPLICATIONS* 12, no. 2 (2018): 403-437. https://doi.org/10.4208/nmtma.OA-2017-0143

[20] Dobrosotskaya, Julia, and Weihong Guo. "A PDE-free variational method for multi-phase image segmentation based on multiscale sparse representations." *Journal of Imaging* 3, no. 3 (2017): 26. https://doi.org/10.3390/jimaging3030026

[21] Zhi, Xu-Hao, and Hong-Bin Shen. "Saliency driven region-edge-based top down level set evolution reveals the asynchronous focus in image segmentation." *Pattern Recognition* 80 (2018): 241-255. https://doi.org/10.1016/j.patcog.2018.03.010

[22] Fang, Lingling, Tianshuang Qiu, Yin Liu, and Chaofeng Chen. "Active contour model driven by global and local intensity information for ultrasound image segmentation." *Computers & Mathematics with Applications* 75, no. 12 (2018): 4286-4299. https://doi.org/10.1016/j.camwa.2018.03.029

[23] Zhao, Wencheng, Xianze Xu, Yanyan Zhu, and Fengqiu Xu. "Active contour model based on local and global Gaussian fitting energy for medical image segmentation." *Optik* 158 (2018): 1160-1169. https://doi.org/10.1016/j.ijleo.2018.01.004

[24] Iqbal, Ehtesham, Asim Niaz, Asif Aziz Memon, Usman Asim, and Kwang Nam Choi. "Saliency-driven active contour model for image segmentation." *IEEE Access* 8 (2020): 208978-208991. https://doi.org/10.1109/ACCESS.2020.3038945

[25] Girija, S. P., A. Akhila, D. Deepthi, R. Uday Kiran, and P. Abinay Krishna. "Saliency and Transmission Feature Extraction from Underwater Images Using Level Set Method." In *2022 First International Conference on Electrical, Electronics, Information and Communication Technologies (ICEEICT)*, pp. 1-7. IEEE, 2022. https://doi.org/10.1109/ICEEICT53079.2022.9768472

[26] Jumaat, A. K., and K. Chen. "Three-dimensional convex and selective variational image segmentation model." *Malaysian Journal of Mathematical Sciences* 14, no. 3 (2020): 437-450.

[27] Bresson, Xavier, Selim Esedoğlu, Pierre Vandergheynst, Jean-Philippe Thiran, and Stanley Osher. "Fast global minimization of the active contour/snake model." *Journal of Mathematical Imaging and vision* 28, no. 2 (2007): 151-167. https://doi.org/10.1007/s10851-007-0002-0

[28] Rudin, Leonid I., Stanley Osher, and Emad Fatemi. "Nonlinear total variation based noise removal algorithms." *Physica D: nonlinear phenomena* 60, no. 1-4 (1992): 259-268. https://doi.org/10.1016/0167-2789(92)90242-F

[29] Chen, Mei-Yun, Yung-Hsiang Yang, Chia-Ju Ho, Shih-Han Wang, Shane-Ming Liu, Eugene Chang, Che-Hua Yeh, and Ming Ouhyoung. "Automatic chinese food identification and quantity estimation." In *SIGGRAPH Asia 2012 Technical Briefs*, pp. 1-4. 2012. https://doi.org/10.1145/2407746.2407775

[30] Lankton, Shawn, and Allen Tannenbaum. "Localizing region-based active contours." *IEEE transactions on image processing* 17, no. 11 (2008): 2029-2039. https://doi.org/10.1109/TIP.2008.2004611

[31] Codella, Noel CF, David Gutman, M. Emre Celebi, Brian Helba, Michael A. Marchetti, Stephen W. Dusza, Aadi Kalloo *et al.,* "Skin lesion analysis toward melanoma detection: A challenge at the 2017 international symposium on biomedical imaging (isbi), hosted by the international skin imaging collaboration (isic)." In *2018 IEEE 15th international symposium on biomedical imaging (ISBI 2018)*, pp. 168-172. IEEE, 2018. https://doi.org/10.1109/ISBI.2018.8363547

[32] Moreira, Inês C., Igor Amaral, Inês Domingues, António Cardoso, Maria Joao Cardoso, and Jaime S. Cardoso. "Inbreast: toward a full-field digital mammographic database." *Academic radiology* 19, no. 2 (2012): 236-248. https://doi.org/10.1016/j.acra.2011.09.014

[33] Shafie, Nur Liyana, and Roslina Mohammad. "Safeguard and mitigation of hazard and operability during simultaneous production and drilling at oil and gas platform." *Progress in Energy and Environment* (2023): 39-49. https://doi.org/10.37934/progee.23.1.3949

[34] Lee, Kiat Moon, and Ka Nyan Ng. "Effect of Ultrasonication in Organosolv Pretreatment for Enhancement of Fermentable Sugars Recovery from Palm Oil Empty Fruit Bunches." *Progress in Energy and Environment* (2019): 15-23.

[35] Yagoub, Sami Abdelrahman Musa, Gregorius Eldwin Pradipta, and Ebrahim Mohammed Yahya. "Prediction of bubble point pressure for Sudan crude oil using Artificial Neural Network (ANN) technique." *Progress in Energy and Environment* (2021): 31-39.